Plasmon Lasers

Wenqi Zhu[1,2], Shawn Divitt[1,2], Matthew S. Davis[1, 2, 3], Cheng Zhang[1,2], Ting Xu[4,5], Henri J. Lezec[1] and Amit Agrawal[1, 2*]

[1]Center for Nanoscale Science and Technology, National Institute of Standards and Technology, Gaithersburg, MD 20899 USA

[2]Maryland NanoCenter, University of Maryland, College Park, MD 20742 USA

[3]Department of Electrical Engineering and Computer Science, Syracuse University, Syracuse, NY 13244 USA

[4]National Laboratory of Solid-State Microstructures, Jiangsu Key Laboratory of Artificial Functional Materials, College of Engineering and Applied Sciences, Nanjing University, Nanjing, China

[5]Collaborative Innovation Center of Advanced Microstructures, Nanjing, China

Corresponding*: amit.agrawal@nist.gov

Recent advancements in the ability to design, fabricate and characterize optical and optoelectronic devices at the nanometer scale have led to tremendous developments in the miniaturization of optical systems and circuits. Development of wavelength-scale optical elements that are able to efficiently generate, manipulate and detect light, along with their subsequent integration on functional devices and systems, have been one of the main focuses of ongoing research in nanophotonics. To achieve coherent light generation at the nanoscale, much of the research over the last few decades has focused on achieving lasing using high-index dielectric resonators in the form of photonic crystals or whispering gallery mode resonators. More recently, nano-lasers based on metallic resonators that sustain surface plasmons – collective electron oscillations at the interface between a metal and a dielectric – have emerged as a promising candidate. This article discusses the fundamentals of surface plasmons and the various embodiments of plasmonic resonators that serve as the building block for plasmon lasers. Based on these concepts, a description of the various experimental implementations of plasmon lasers is given, the characteristic parameters that describe their performance are highlighted, and the potential applications of plasmon lasers are discussed.

1. Introduction:

The field of plasmonics studies the collective electron oscillations in a metallic medium ("plasmons") and their interactions with external electromagnetic fields ("polaritons"). Plasmon polaritons are electromagnetic fields that are bound to a metal-dielectric interface and have been historically categorized into two types: *surface plasmon polaritons* (SPPs) and *localized surface plasmons* (LSPs), where SPPs refer to propagating polaritons that travel along a metal-dielectric interface, and LSPs refer to oscillations of electrons that are bound to the enclosed surface of an isolated metallic nanostructure.

The field of plasmonics, as a fundamental part of the larger field of nanophotonics, has undergone tremendous development during the past several decades thanks to the flexibility in engineering the characteristics properties of a plasmon. For example, the dispersion properties of propagating SPPs can be readily controlled, leading to interesting phenomena such as extraordinary optical transmission [1], negative index of refraction [2], and "spoof" surface plasmons [3], leading to applications such as nano-lasing [4], nano-circuitry [5], and collimation of surface emitting lasers [6]. On the other hand, the absorption and scattering properties of metallic nanoparticles that exhibit LSP resonances can be engineered by controlling the particle size, geometry, constituent material and surrounding medium, leading to their applications as solar cells [7], optical filters [8], and building blocks for metamaterials and metasurfaces [9, 10]. The enhancement of electromagnetic field intensity in the vicinity of the nanoparticle enabled by LSP resonances has also led to applications in single-molecule detection [11], optical trapping of bacteria and biological tissues [12], and nonlinear optical conversion at the nanoscale [13].

Both SPPs and LSPs can undergo stimulated emission, which naturally leads to devices that are the plasmonic analogue of lasers, known simply as *plasmon lasers*. Plasmon lasers represent a major research effort in implementing nanoscale, coherent light sources with ultra-small optical mode volumes. Such devices show promise in biosensing, on-chip optical communications, and ultrafast manipulations of light-matter interactions. This encyclopedia article gives a description of the physics and performance metrics of plasmon lasers, as well as their potential applications. The description begins in summarizing the fundamental physics associated with SPPs and LSPs, highlighting the necessity and challenges of implementing a plasmon laser. Then, various types of plasmonic resonant cavities that serve as the building block for plasmon lasers are summarized. Based on these concepts of surface plasmons and plasmon resonators, the various experimental implementations of plasmon lasers to date is discussed, along with a summary of their characteristic performance.

2. Fundamentals of Surface Plasmons

2.1 Drude-Sommerfeld model of metals

This section begins with the modeling of "volume" plasmons – electron oscillations within a metal. More specifically, an illustration is given of the collective response of free-electrons subject to a source electromagnetic field, using a Lorentzian oscillator model. In Figure 1a, a static electric field E_0 is applied to an opaque, infinitely large metal block, creating net charge densities $\pm neu_z$ displaced by distance u_z, where e is the electron charge and n is the free charge density of the metal. Once E_0 is turned off, allowing the positive charge densities to create a driving force on a given free electron, the free electron will start an oscillation motion as is described by:

$$\frac{d^2u_z}{dt^2} = -\frac{e}{m^*}E_z \tag{2.1.1}$$

where m^* is the effective mass of the electron; $E_z = neu_z/\varepsilon_0$ is the driving field as induced by the positive charge densities; and ε_0 is the free-space permittivity. Inserting the expression for E_z into equation (2.1.1) gives

$$\frac{d^2u_z}{dt^2} = -\omega_{\mathrm{res}}^2 u_z \quad , \tag{2.1.2}$$

where the resonance frequency ω_{res} represents the natural collective oscillation of electrons in the volume (hence known as "volume" plasmon) of a metal. ω_{res} of volume plasmons is traditionally referred to as the plasma frequency ω_{p}, which is expressed as

$$\omega_{\mathrm{p}} = \sqrt{\frac{ne^2}{m^*\varepsilon_0}} \quad . \tag{2.1.3}$$

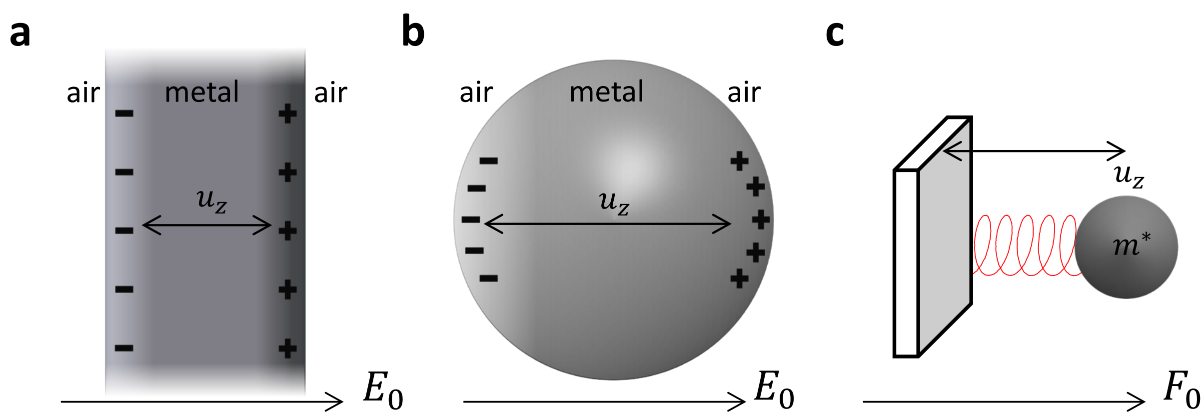

Figure 1 | A classical description of plasmons as collective oscillations. a, A static field E_0 applied to a thin metallic film surrounded by air. **b,** A static field E_0 applied to a spherical metallic particle surrounded by air. **c,** The oscillation of a single electron with charge e in an electric field E_0 is represented by a damped oscillator experiencing a driving force $F_0 = eE_0$.

The surface geometry of a metal also plays a role in determining the collective free electron oscillation frequency inside the metal. Figure 1b illustrates this scenario using the example of a spherical metallic particle. The polarization density response to the applied static field E_0 in this scenario is calculated as $P_z = -neu_z$, which in turn creates the response field $E_z = -P_z/3\varepsilon_0$. Inserting this into equation (2.1.1) results in a new expression for the surface plasmon resonance frequency given by $\omega_{\text{res}} = \omega_{\text{p}}/\sqrt{3}$. In general, however, the relationship between plasmon resonance and geometry is non-trivial, and as discussed in Sections 2.2 & 2.3, the dielectric environment also influences these resonances.

Now consider the effect that free-electrons in a metal can scatter from the background positive-ion lattice structure, resulting in a damped oscillation motion for the electrons. This is represented by the inclusion of a damping factor γ in equation (2.1.1). The dynamics of the free-electrons in the presence of damping and a time harmonic driving field $\vec{E}_0 e^{-i\omega t}$ is given by:

$$\partial_t^2 \vec{u} + \gamma \partial_t \vec{u} = -\frac{e}{m^*} \vec{E}_0 e^{-i\omega t} \quad . \tag{2.1.4}$$

This damped oscillator model of the free-electron response is illustrated in Figure 1c. Macroscopic material parameters are derived using expressions for both the polarization density $\vec{P} = \varepsilon_0(\varepsilon - 1)\vec{E}_0 = ne\vec{u}$ and electric flux density $\vec{D} = \varepsilon_0 \varepsilon \vec{E}_0 = \varepsilon_0 \vec{E}_0 + \vec{P}$. Inserting a time harmonic expression for the amplitude oscillations $\vec{u} = \hat{u} u e^{-i\omega t}$ into equation (2.1.4), and substituting in the polarization density and electric flux density, results in the Drude-Sommerfeld expression for the permittivity of a damped plasma, given by:

$$\varepsilon(\omega) = \varepsilon_\infty - \frac{\omega_{\text{p}}^2}{\omega^2 + i\gamma\omega} \quad . \tag{2.1.5}$$

Interband transitions occurring when $\omega > \omega_{\text{p}}$ are accounted for with the inclusion of the constant ε_∞ in equation (2.1.5). The dielectric function is complex and is written as $\varepsilon(\omega) = \varepsilon'(\omega) +$

$i\varepsilon''(\omega)$ for real numbers $\varepsilon'(\omega)$ and $\varepsilon''(\omega)$. For typical plasmonic metals such as Au, Ag, or Al, at optical frequencies, both $\varepsilon'(\omega) < 0$ and $|\varepsilon'(\omega)| \gg |\varepsilon''(\omega)|$ when $\omega < \omega_\mathrm{p}$ is satisfied. These properties, along with specific surface geometries, determines the properties of the excited propagating or localized surface plasmons. The next two sections will discuss the conditions for exciting these two categories of surface plasmon modes.

2.2 Propagating SPPs on a planar metal/dielectric interface

Figure 2a illustrates a transverse-magnetic (TM) plane wave at optical frequencies incident from one medium to another at the Brewster angle θ_B, with the interface placed at $z = 0$. Each medium is non-magnetic and described by dielectric constants ε_m for regions $m = 1, 2$. Additionally, the spatial frequencies in each region obey the relationship $\varepsilon_m k_0^2 = k_x^2 + k_{m,z}^2$ where $\vec{k}_m = \hat{a}_x k_x + \hat{a}_z k_{m,z}$. The plane-wave solutions for regions $m = 1, 2$ are:

$$\vec{\mathrm{H}}_m = \hat{a}_y \mathrm{H}_m e^{i(k_x x + k_{m,z} z)} \quad . \tag{2.2.1a}$$

$$\vec{\mathrm{E}}_m = \frac{-i\mathrm{H}_m}{\omega \varepsilon_0 \varepsilon_m} \left(\hat{a}_x k_{m,z} + \hat{a}_z k_x\right) e^{i(k_x x + k_{m,z} z)} \quad . \tag{2.2.1b}$$

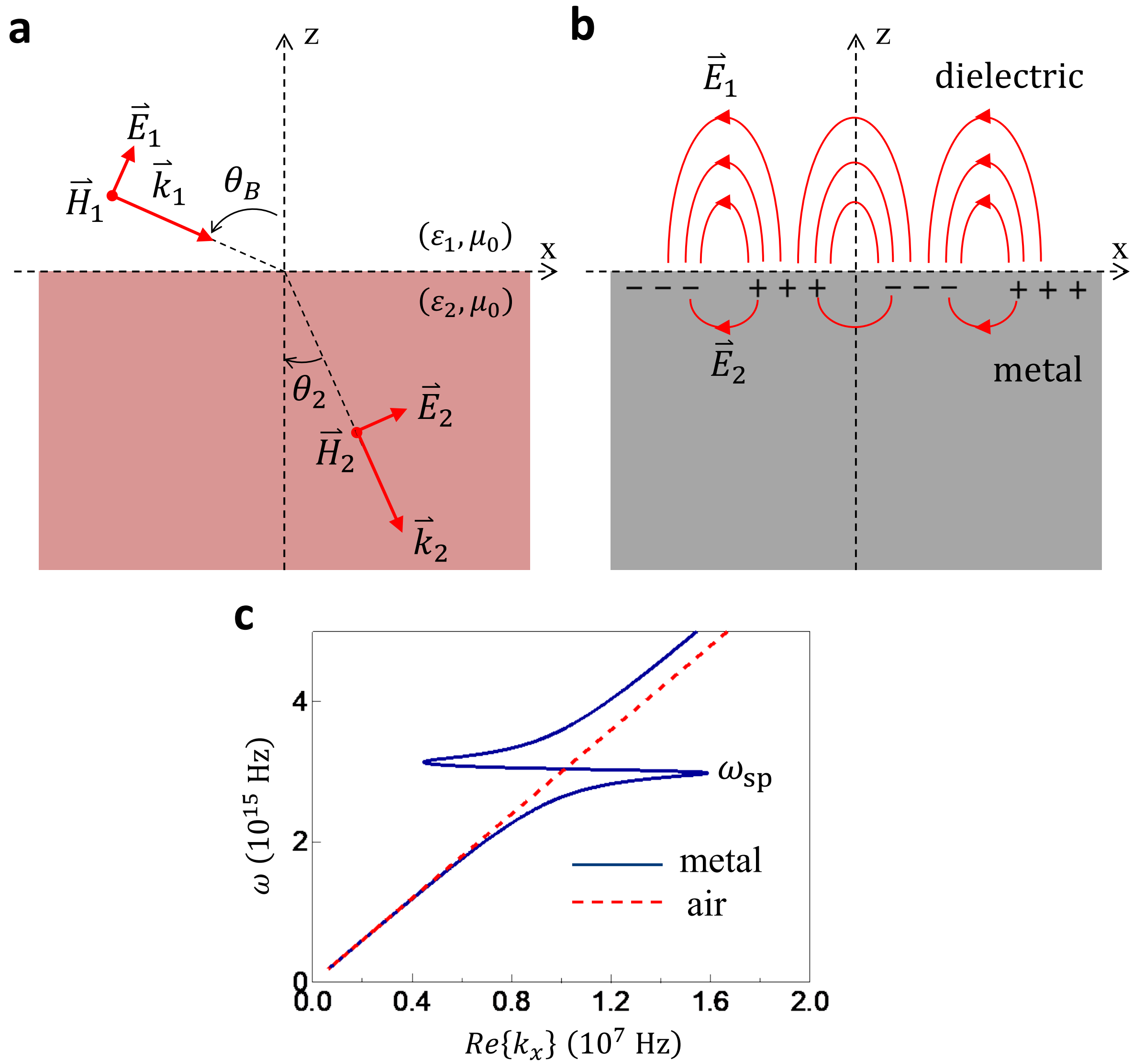

Figure 2 | Surface-plasmon-polariton modes a, A transverse magnetic (TM) polarized plane wave is incident from medium 1 having material parameters (μ_0, ε_1) onto medium 2 having parameters (μ_0, ε_2) at the Brewster angle θ_B. Both dielectric media are homogeneous, isotropic, and non-magnetic. Note that $\theta_B + \theta_2 = \pi/2$. **b,** If medium 1 is a dielectric and medium 2 is a metal, the Brewster angle condition results in SPP resonant modes. **c,** The SPP (blue-solid line) and free-space (red-dashed line) dispersion curves. When the frequency is smaller than ω_{sp}, the two curves diverge, with the SPP curve representing a wave bound to a surface. For frequencies beyond ω_{sp}, the modes are no longer SPP modes as they are not bound to the surface.

Maxwell's equations dictate the field expressions in equation 2.2.1 and obey the relationships $\vec{E}_1 \cdot \hat{a}_x = \vec{E}_2 \cdot \hat{a}_x$ and $\varepsilon_1 \vec{E}_1 \cdot \hat{a}_z = \varepsilon_2 \vec{E}_2 \cdot \hat{a}_z$ across the interface at $z = 0$ [14]. Applying these conditions to equations 2.2.1a-b results in $H_1 k_{1,z}/\varepsilon_1 = H_2 k_{2,z}/\varepsilon_2$ and $H_1 = H_2 = H_0$ for a real constant H_0. These two expressions then give the relation,

$$\frac{k_{1,z}}{\varepsilon_1} = \frac{k_{2,z}}{\varepsilon_2} \quad . \tag{2.2.2}$$

Combining equations (2.2.2) with $\varepsilon_m k_0^2 = k_x^2 + k_{m,z}^2$ for $m = 1, 2$, where k_0 is the free-space wavenumber of the field, produces the dispersion relation,

$$k_x^2 = \frac{\varepsilon_1 \varepsilon_2}{\varepsilon_1 + \varepsilon_2} k_0^2 \quad , \tag{2.2.3a}$$

$$k_{m,z}^2 = \frac{\varepsilon_m^2}{\varepsilon_1 + \varepsilon_2} k_0^2 \quad . \tag{2.2.3b}$$

Equations (2.2.3a-b) are the dispersion relations for the Brewster condition, however if medium 1 is a dielectric described by a real-valued dielectric constant, and medium 2 is a metal with a dielectric constant described in the previous section, then the following relationship represents a resonance condition resulting in surface-plasmon-polariton (SPP) modes:

$$\varepsilon_1(\omega)\varepsilon_2'(\omega) < 0 \quad , \tag{2.2.4a}$$

$$\varepsilon_1(\omega) + \varepsilon_2'(\omega) < 0 \quad . \tag{2.2.4b}$$

Under these conditions, the spatial frequency components become complex in both media, resulting in $k_x = k_x' + ik_x''$ for real values of k_x' and k_x'', and $k_{m,z} = k_{m,z}' + ik_{m,z}''$ for real values of $k_{m,z}'$ and $k_{m,z}''$. For many dielectric/metal interfaces the approximation $k_{m,z} \approx ik_{m,z}''$ is used

[15]. The result is a wave that propagates along the interface at $z = 0$ and exponentially decays normal to the surface. The SPP wave expression is:

$$\vec{H}_{\mathrm{SPP}} = \hat{a}_y H_0 e^{ik'_x x} e^{-(k''_x x + k''_{m,z} z)} \quad . \tag{2.2.5}$$

Figure 2b suggests that an SPP is a surface wave that is bound to and propagates along the metal-dielectric interface. The electromagnetic field intensity decays exponentially away from the surface, indicating a subwavelength scale mode volume – a property that is desired for a nanoscale laser as discussed in Section 4.3(v). On the other hand, the presence of the term k''_x in equation (2.2.5) suggests energy is dissipated in the metal as the SPP propagates – the loss channel that limits the quality factors of plasmonic resonators (Section 3.1) and needs to be compensated to achieve lasing (Section 4.3(ii)).

Along the SPP propagation direction, the effective SPP wavelength λ_{SPP} is also subwavelength: this is observed in the k'_x term of equation (2.2.5) via $\lambda_{\mathrm{SPP}} = 2\pi/k'_x$, and in general $\lambda_{\mathrm{SPP}} < \lambda$. Figure 2c shows the SPP mode and free-space dispersion curves for a medium using parameter values in equation (2.1.5) typical of metals such as $\gamma = 10^{14}$ Hz, $\omega_{\mathrm{p}} = 10^{16}$ Hz, and $\varepsilon_\infty = 10$ [16]. At low optical frequencies, both curves nearly touch. This is the region of the grazing Sommerfeld-Zenneck surface waves [16]. As the optical frequency increases, the two dispersion curves diverge and special techniques are required to couple incident light to SPP modes [15, 16]. The SPP *k*-vector reaches a maximum at the surface plasmon frequency ω_{sp}. Assuming medium 1 is air, the surface plasmon frequency is given by $\omega_{\mathrm{sp}} = \omega_{\mathrm{p}}/\sqrt{1+\varepsilon_2}$. Although the free-space light is confined to smaller wavelengths as the *k*-vector increases, the damping loss, in addition to a decrease in group velocity, limits the effective SPP propagation length to the order of 10 μm [16]. SPP modes are no longer accessible as the optical frequency increases beyond ω_{sp}.

For very large frequencies, the medium loses its metallic properties and its dispersion curve once again follows the light-line.

2.3 Localized surface plasmon (LSP) resonances

Now consider the case for LSPs, which are non-propagating surface plasmon modes confined by the geometry of a metal nanoparticle.

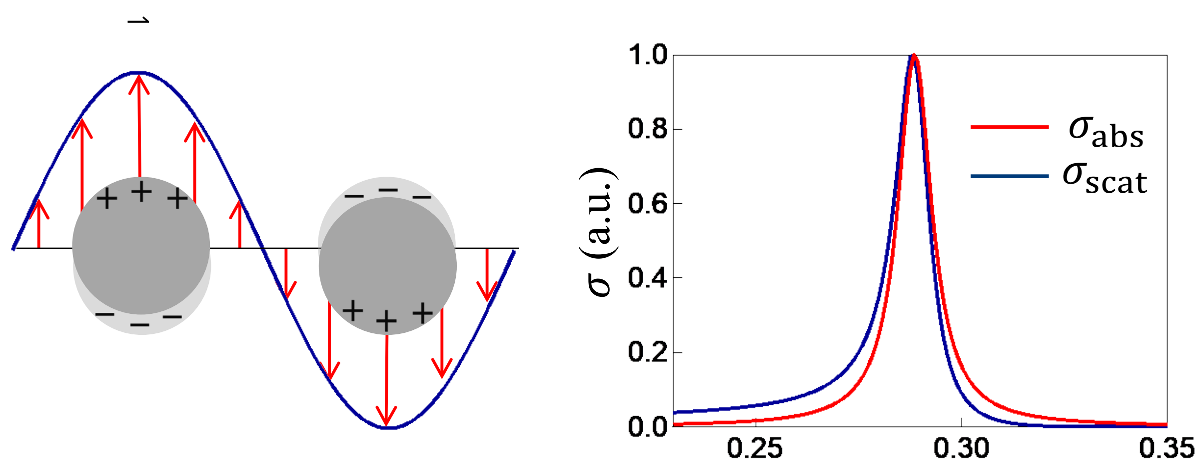

Figure 3 | Localized surface plasmon resonant modes a, A plane wave with wavelength λ is incident from a dielectric medium onto a non-magnetic metallic particle with radius a. The particle radius is small compared to the wavelength, $a \ll \lambda$. **b**, The absorption and scattering cross sections of a spherical metal nanoparticle. The peaks in the curve indicate the presence of LSP modes.

In Figure 3a, an electromagnetic plane wave with wavelength λ is incident on a spherical metal particle with radius $a \ll \lambda$. The electromagnetic field induces an electric-dipole moment $\vec{p} = \alpha \vec{E}_1$, where α is the polarizability of the metal particle. For a spherical particle, the polarizability takes the form [17]:

$$\alpha = 4\pi\varepsilon_0 a^3 \frac{\varepsilon_2 - \varepsilon_1}{\varepsilon_2 + 2\varepsilon_1} \quad . \tag{2.3.1}$$

The scattering and absorption cross-sections for a spherical particle are then given by:

$$\sigma_{\text{scat}} = \frac{k^4}{6\pi}|\alpha|^2 \quad , \tag{2.3.2a}$$

$$\sigma_{\text{abs}} = k\text{Im}(\alpha) \quad . \tag{2.3.2b}$$

Figure 3b illustrates these cross-sections for the same metal and dielectric parameters used to calculate the dispersion curve in Figure 2c. The peak amplitudes occur when $Re\{\varepsilon_2 + 2\varepsilon_1\} = 0$: the resonance condition for exciting LSP modes. As discussed in Sections 3(iii) & 4.2(i), nanoscale particles can act as self-contained resonators for the amplification of LSP modes in a gain medium, and therefore can serve as a useful ingredient in the development of deep-subwavelength nano-lasers.

3. Plasmonic Cavities

Stimulated emission is typically achieved using an optical resonator, and plasmon lasers are no exception. In this section, several embodiments of surface plasmon resonators are discussed.

(i) Plasmonic Fabry-Perot cavities. As described in Section 2.2, SPP is a wave that propagates along a metal-dielectric interface. Reflective surfaces can be used to form cavities for SPPs, where the waves are reflected between the surfaces, resulting in a Fabry-Perot type cavity for SPPs. For certain wavelengths, a standing-wave forms inside the cavity, corresponding to a resonant condition. A measure for the relative strength of the resonance is known as the quality factor (*Q*-factor):

$$Q = {}^{\lambda}/_{\delta\lambda} \quad , \tag{3.1.1}$$

where λ is the resonance center wavelength and $\delta\lambda$ is the resonance linewidth. The cavities themselves typically need to be *stable*, where the reflected waves will stay within the cavity even after many reflections.

Plasmonic Fabry-Perot cavities have been demonstrated for both wedge waveguides and planar waveguides. For the wedge waveguide cavity, wedge-plasmon polariton resonators are formed at the ridge of a long triangular wedge. The ridge acts as a one-dimensional (1-D) waveguide along which the SPP waves propagate. Metal strips are placed at positions along the wedge that act as high reflectors. Resonators with a Q-factor > 190 have been achieved in the visible spectrum using template stripped Ag surfaces [18]. For SPPs existing on a planar metal film, both curved and flat reflectors have been successfully employed in building plasmonic Fabry-Perot cavities. An example of such a cavity along with a typical far-field spectrum are shown in Fig. 4a and 4b respectively. The earliest successfully demonstrated planar resonator is a Fabry-Perot resonator created by Sorger *et al.*, who formed a long trench between two vertical silver reflectors [19]. This original design has been subsequently improved upon, such that Q-factors as high as 310 have been successfully demonstrated in the visible region of the electromagnetic spectrum [20]. Curved metallic mirrors can also been used to generate planar resonators with comparably high Q-factors [21]. It is worth noting that higher-order hybrid-photonic-plasmonic modes can exist within these planar resonators, but fundamental SPP modes can be singled out by controlling the height of the reflectors.

(ii) Gap plasmon cavities. When an SPP wave reaches the edge of a dielectric or semiconductor facet, a portion of the wave will be reflected back due to Fresnel reflections. Such a reflection can be employed in place of a cavity mirror to form a resonator (Fig. 4c). An early demonstration is by

Oulton *et al*., who exploited this concept to construct a gap plasmon cavity [4]. Here, the gap plasmon refers to the plasmonic mode confined in between a planar metal film and a high-index semiconductor nanowire. The large refractive index of the semiconductor material naturally provides a large reflection coefficient at the end facet. A 2-dimensional cavity (Fig. 4d) can also be formed by replacing the nanowire with a nano-slab [22].

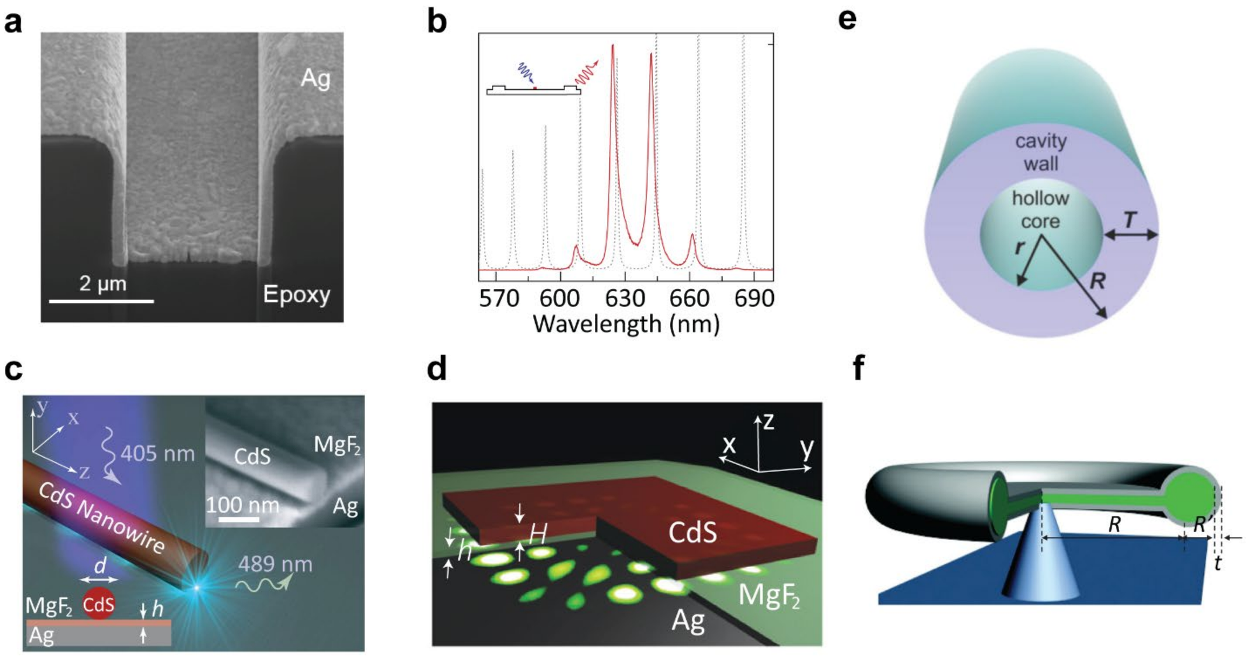

Figure 4 | Surface plasmon polariton cavities. a, Cross-section of a planar Fabry-Perot cavity with two planar end mirrors. Reprinted from [20]. © The Authors, some rights reserved; exclusive licensee American Association for the Advancement of Science. Distributed under a Creative Commons Attribution NonCommercial License 4.0 (CC BY-NC). **b**, Measured (red solid line) and simulated (gray dashed line) resonance spectrum of a plasmonic Fabry-Perot resonator. Adapted from [21]. **c,** Schematic diagram of a dielectric-fact cavity that supports plasmonic-photonic-hybrid modes. This cavity consists of a semiconductor nanowire and a planar metal film, separated by a nanoscale dielectric gap. Adapted from [4]. **d,** Schematic diagram of a two-dimensional (2-D) dielectric-facet cavity which consists of a semiconductor nanodisk and a planar metal film, separated by a nanoscale dielectric gap. Adapted from [22]. **e,** Schematic diagram of a metal-coated plasmonic cylinder that can support plasmonic whispering-gallery modes. **f,** Schematic diagram of a plasmonic toroidal cavity. Adapted from [25].

(iii) LSP open-cavities. As discussed in Section 2.3, free electrons within an isolated metallic nanoparticle can undergo a collective oscillation known as LSP, which is a quantum of localized electron plasma oscillation. Similar to other oscillators, resonance plays a role in the amplitude and decay time of LSPs. In general, the resonant frequency of the LSP depends on the material, size, shape, and local environment of the particle [23]. The sensitive dependence of LSPs on their local environment has been exploited in applications such as refractive index sensing [24], surface-enhanced Raman scattering (SERS) [25], and tip-enhanced Raman scattering (TERS) [26].

As discussed in Section 2.3, analytical solutions for LSPs exist in the case of spherical particles. These solutions remain valid through deep sub-wavelength scales until a quantum mechanical treatment becomes necessary. Quasi-analytical solutions exist for non-spherical particles, including the multiple-multipole method and the volume integral method [15]. Purely numerical methods are also applicable, including finite-difference time-domain methods.

Typical experiments that exploit LSP resonances use silver (Ag) or gold (Au) nanoparticles. Ag and Au offer LSP resonances that fall within the visible spectrum with reasonably high Q-factors (10 to 40). Ag nanoparticles typically offer resonances in the blue region with higher quality factors than that of Au nanoparticles, while Au nanoparticles are less prone to undergo chemical changes in experimental ambient environmental conditions. Given a local gain medium and sufficient excitation power, LSP resonances can also undergo a transition into lasing behavior (see Section 4).

(iv) Lattice plasmon cavities. A different type of resonance emerges in quasi-infinite arrays of single LSP resonators, known as delocalized "lattice plasmons", surface Bloch modes, or surface lattice resonances [27-29]. Individual resonators that are separated by a dielectric medium can be coupled by a scattered, in-plane electromagnetic field and undergo coherent oscillation [30]. In this case, the electromagnetic field is delocalized from the individual particles and can lead to resonances with much higher Q-factors than those of any individual particle because of reduced metallic absorption. Such resonances have also been shown in cases where a plasmonic crystal lattice can be formed [31].

(iv) Hybrid-photonic-plasmonic cavities. Generally, the cavities that support resonant hybrid-photonic-plasmonic modes can also be defined as plasmonic cavities. These hybrid modes have an SPP-like field at the surface of the metal and photon-like fields inside the dielectric. Instead of using reflection at interfaces to form a standing wave inside the cavity, a ring-shaped cavity such as toroid or cylinder can be used such that waves traveling in both the clockwise and counterclockwise directions form a standing wave, given the proper wavelength. Waves of this type are typically known as whispering-gallery waves. One of the few analytically tractable resonators is the infinitely extended cylinder (Fig. 4e). A metal-coated dielectric cylinder can carry SPPs on both the inner and outer metal interfaces. The SPP mode on the inner surface typically has a much higher Q-factor than that on the outside, which can reach 700 at the red end of the visible spectrum [32, 33]. Hybrid modes generally exist in a single-dielectric cylinder, which can lead to a very large number of simultaneously excited modes for cylinders with a large radius. Toroidal resonators are also capable of carrying SPPs with a high Q-factor (Fig. 4f). Here, the SPP propagates along the length of the tube and not around the circumference. Theoretically, these resonators can support an SPP mode on the outer surface with a Q-factor of 1000 at the red-end of the spectrum [34].

4. Plasmon Lasers

LASER is the acronym for 'light amplification by stimulated emission of radiation'. The development of various types of lasers since their inception in the 1960s has revolutionized the field of optics by providing coherent, high intensity light sources on demand. This section focuses on one sub-category of lasers which achieves stimulated light emission in the form of surface plasmons. These devices are known as SPASERs or plasmon lasers and represent a major effort in implementing nanoscale light sources that exploit the subwavelength optical confinement offered by surface plasmons. In this section, the concepts and implementations of plasmon lasers are discussed and the characteristic parameters that govern their performance are summarized. Some practical applications of plasmon lasers are also highlighted.

4.1 Plasmon lasers *vs.* Photonic/Hybrid lasers

Analogous to conventional lasers, a plasmon laser consists of a medium that provides an optical gain and a cavity that supports a resonant mode of a surface plasmon. The stimulated emission of a surface plasmon is achieved when the optical gain from the gain medium compensates the loss of the cavity. The semi-classical model of a plasmon laser, shown in Fig. 5a, describes such an optical process, where a three-level gain medium provides an optical gain that allows the stimulated emission of SPPs in a resonant plasmonic cavity [35]. Based on this semi-classical model, the build-up of lasing action can be numerically simulated in the time domain by combining the rate equation of the gain medium with a finite-difference time-domain method that simulates the plasmon resonance [28]. A complete quantum mechanical model has also been used to examine the coherence characteristics of the waves emitted by a plasmon laser [36].

Compared to lasing based on photonic modes or hybrid-photonic-plasmonic modes, a pure plasmonic mode lasing faces a bigger challenge as the quality factors of plasmonic cavities are typically smaller than those of photonic or hybrid cavities. However, achieving plasmonic mode lasing can be desirable because of the high confinement of the electromagnetic field near the metal surface, which allows for sensitive refractive index sensing and enables nanoscale optical devices with enhanced light-matter interactions. The enhanced interaction between the plasmonic mode and the gain medium also contributes in reducing the lasing threshold of specific types of plasmon laser. Moreover, the miniaturization provided by plasmonic devices is also beneficial, which stems from the typically smaller wavelength of SPPs relative to photonic modes with the same frequency. For example, electro-optic modulators with nanometer size and extremely high speed are enabled by SPPs [37] where photonic modes are inferior due to their large wavelength and weak electric field enhancement.

4.2 Plasmon laser implementations

Several terms exist for referring to plasmon lasers in the research community, including SPASERs, gap/lattice plasmon lasers, and surface plasmon polariton lasers. Despite the common character of achieving stimulated emission of surface plasmons, the above terms have been used to differentiate specific plasmonic modes that resonate inside plasmonic cavities of different geometries. These different implementations of plasmon lasers are placed into the following categories.

(i) SPASERs. The term "SPASER" hints at a broad range of plasmon lasers, but it is most commonly used to describe devices which achieve lasing of localized surface plasmons (LSPs). The first model-prototype of a SPASER was theoretically proposed in 2004, which consists of colloidal Ag nanoshells coated with fluorescent nanocrystals serving as the gain medium (Fig. 5b) [38]. Such a configuration can be viewed as an open cavity laser where the optical mode is not confined by any mirrors; instead, the lasing is based on the LSP resonances of individual plasmonic nanoparticles. The first experimental implementation of a SPASER was reported in 2009 [39], where colloidal Au nanospheres were enclosed by laser-dye doped polymers. These polymers can provide optical gain when pumped with a sequence of nanosecond optical pulses. Lasing action was claimed based on observations of threshold pump-power for laser emission, enhanced photon decay rate, and linewidth narrowing of the emitted light. The major benefit of a SPASER is its extremely small mode volume. However, in this first experiment the observed linewidth was on the order of 5 nm, leading to skepticism of its degree of temporal coherence [36]. This large emission linewidth is directly related to the low Q-factor of the localized surface plasmon resonances due to metallic absorption and optical radiation loss.

(ii) Lattice plasmon lasers. Parallel to the effort with individual particles, another type of SPASER was proposed and implemented based on a periodic lattice of plasmonic nanoparticles. As discussed in Section 3.2, such a periodic arrangement of nanoparticles constitutes an LSP resonator array. The "lattice plasmon" modes, referring the Bloch mode of the plasmonic lattice, exhibit a higher Q-factor than those of individual plasmonic nanoparticles. In its original design in 2007 [40], plasmonic split ring resonators were employed to build the array. The LSP resonance of individual split ring resonators at the microscopic scale form a dark mode with minimal radiation losses and create an "open" cavity for the SPASER (Fig. 5c). Further experimental efforts showed that similar lasing action can be achieved in an array of plasmonic nanodisks or nanoholes that support sub-radiant dark plasmon modes [28, 41]. The Q-factors of these lattice plasmon modes can be as large as ≈ 200, which significantly reduces the amount of optical gain needed to achieve lasing. Both semiconductor and laser dye materials have been used as the optical gain medium in SPASERs together with a pulsed pump laser. Experimental characterizations show that lattice plasmon lasers arrays exhibit higher temporal and spatial coherence compared to those based on randomly arranged individual plasmonic nanoparticles, with a lasing emission linewidth as narrow as ≈ 0.2 nm and a collimated emission pattern. One drawback of SPASERs based on resonator arrays is that their length scale is on the order of tens of microns.

(iii) Gap plasmon lasers. The first demonstration of a plasmon laser was reported in the form of gap plasmons in 2009 [4]. In this design, a direct-bandgap cadmium sulfide semiconductor nanowire, which served as the optical gain medium, was brought near a planar metal film (Fig. 4c). A thin dielectric layer was used to separate the nanowire from the metal film. Such a geometry supports a gap mode whose field maximum is located at the metal-dielectric interface and decays exponentially into the metal layer, exhibiting characteristics of a plasmon mode. The presence of the semiconductor nanowire, typically with a large refractive index, further confines this plasmon mode to the deep-subwavelength-scale gap. The two end-facets of the nanowire function as two end-mirrors to form a Fabry-Perot-like cavity, giving Q-factors of ≈ 100. The lasing action was first achieved at cryogenic temperatures under optical pumping with femtosecond optical pulses (Fig. 5d). Because of the high damage threshold of semiconductor materials, the laser was able to work stably in the linear regime, demonstrating the capability of practical applications such as a nanoscale coherent light source. Following this initial work, the performance of plasmon lasers has been dramatically improved in various aspects, including in the emission linewidth, lasing temperature, and modulation speed [22, 42]. The design has also been extended to plasmon lasers in the ultraviolet region [43].

(iv) SPP lasers. As discussed in Section 2, the primary loss mechanism for propagating SPPs is the metal absorption at optical frequencies. Therefore, significant efforts have been devoted to demonstrating lasing from SPPs by exploiting Fabry-Perot-like resonant cavities. These implementations of plasmon lasers are often termed *SPP lasers*. As discussed in Section 3, a simple Fabry-Perot cavity for propagating SPPs consists of a planar metal film and two high-reflectivity mirrors (Fig. 5e). Quality-factors up to 500 for micron-scale cavity lengths can be achieved, which are among the largest reported for planar SPPs. By incorporating laser dye molecules into these low-loss cavities, plasmon lasing action was observed with threshold behavior and narrowing of emission linewidth under optical pumping with nanosecond pulses [20, 21]. The demonstrated pumping threshold intensity of these lasers is much lower than those of SPASERs using similar optical gain media due to the comparatively higher Q-factor. Emission linewidths of 0.2 nm have been achieved.

One drawback of propagating surface plasmon lasers, as discussed in Section 3.1.1, is that hybrid and purely photonic modes can co-exist in the same cavity, which may be undesirable. Luckily, in the case of the semiconductor-nanowire plasmon lasers, the photonic modes inside the wire typically have a much higher lasing threshold than the gap plasmon mode. In the case of the Fabry-Perot type plasmon lasers, photonic modes can be filtered out by careful selection of the gain medium thickness and reflector height.

(v) Others. Various types of lasing actions have been proposed or observed that are related to plasmonic effects. In these studies, the general goal is to achieve coherent radiation within the plasmonic modes of interest. For example, *metamaterials* is a research field that is closely related to plasmonics. Lasing action in hyperbolic metamaterials has been shown through the incorporation of optical gain media [44]. Another example is a 'mirror-free' nano-laser that relies on a backward-travelling plasmon mode inside a metal-insulator-metal waveguide, which confines the light at the nanoscale [45].

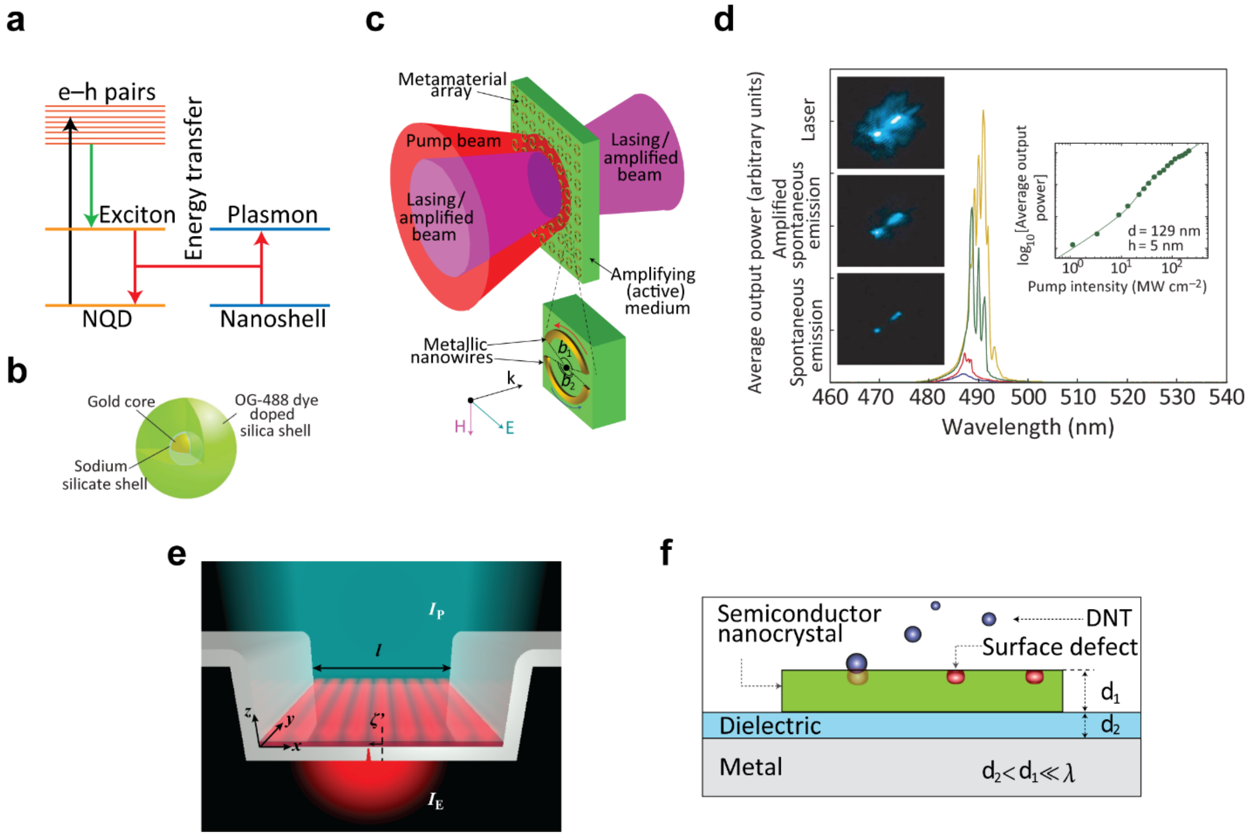

Figure 5 | Concept and examples of plasmon lasers. a, Semi-classical model description of a plasmon laser. The optical gain provided by the exciton can support the stimulated emission of plasmons. Adapted from [35]. **b**, A typical SPASER implementation showing individual plasmonic nanoparticles coated with optical gain medium. Adapted from [38]. **c,** Schematic diagram of a planar plasmon laser design which consists of a 2-D array of subradiant plasmonic nanostructures. Adapted from [39]. **d,** Example of plasmon laser emission spectra. The spectra are measured at different pump powers. Inset images, micrograph images of the plasmon lasers under different pump powers. Inset figure, emission power as the function of pump power. Adapted from [4]. **e,** Schematic diagram of the metallic trench SPP laser, consisting of a gain medium-decorated Fabry-Perot resonator, illuminated with a pump beam (blue-green). The schematic standing wave (red) illustrates a trapped SPP lasing mode. Reprinted from [20]. © The Authors, some rights reserved; exclusive licensee American Association for the Advancement of Science. Distributed under a Creative Commons Attribution NonCommercial License 4.0 (CC BY-NC). **f,** Schematic diagram of an active dielectric sensing design based on a plasmon laser. Adapted from [50].

4.3 Performance characteristics of plasmon lasers

Among plasmon lasers, there is not yet a universal design that outperforms others in every performance characteristic. This is because a plasmon laser is usually designed to emphasize a particular aspect of laser characteristic performance. In the following, a summary is given of typical performance characteristics for the plasmon lasers that have been reported. Also provided is a general guidance on the type of plasmon laser that should be chosen for a given application.

(i) Lasing wavelength. Plasmonic effects associated with noble metals are mostly discussed in the wavelength range between ultraviolet and infrared. Plasmon lasing with emission wavelengths spanning this range have been achieved by selecting appropriate plasmonic cavities and optical gain media. In particular, ultraviolet and blue plasmon lasers with wavelengths from 370 nm to 500 nm are made possible with gap plasmon lasers using appropriate direct-bandgap semiconductor nanowires [4, 22, 43]. Plasmon lasers working in the telecommunications band have also been made possible by patterning plasmonic structures on semiconductor substrates [41]. For wavelengths between green and near-infrared regimes, various laser dye molecules and fluorescent quantum dots are commonly used as the optical gain media, although dye molecules in particular show short lifetimes [46]. These gain media are easily brought in proximity with plasmonic resonators to provide maximum modal gain. Ag and Au are the most common materials in plasmonic cavities because of their low absorption coefficient in visible and infrared whereas Al is typically employed for plasmon laser operation in the ultraviolet [43].

(ii) Lasing threshold. Direct-bandgap semiconductors and laser dyes are the most commonly used optical gain media for plasmon lasers. In all implementations reported to date, optical pumping using a femtosecond or nanosecond pulse is required. Neither continuous wave (CW) pumping nor electrical pumping of plasmon lasers has yet been achieved. In the case of plasmon lasers using dyes, the minimum lasing threshold, defined as the average intensity of the pumping beam, is ≈ 10 MW/cm^2. This was observed in a propagating SPP laser with a large *Q*-factor [20]. Continuous replenishment the laser dye molecules is necessary to extend the lifetime of these devices. For lasers using direct-bandgap semiconductors, the lasing threshold is ≈ 3.5 MW/cm^2 for cryogenic temperature measurements and ranges from 10 MW/cm^2 to 60 MW/cm^2 for room temperature measurements. However, because of the high damage threshold of the semiconductor materials and immunity to photobleaching, these lasers usually have long lifetimes, making them suitable for practical applications.

(iii) Temporal coherence. In the majority of work reported to date, the temporal coherence of stimulated emission of surface plasmons is inferred by observing the linewidth narrowing of the scattered light. For SPASERs, the achieved emission linewidth has been improved from ≈ 5 nm in its first demonstration to ≈ 0.2 nm in the most recent work, thanks to the improved *Q*-factor of the plasmonic cavity and a microfluidic channel that replenishes the laser dyes [28, 47]. SPP lasers exhibit even narrower emission linewidths down to 0.16 nm, due to the higher *Q*-factors of the Fabry-Perot cavities for the plasmon modes.

(iv) Spatial coherence. Spatial coherence is an important parameter for bulk semiconductor lasers such as distributed-feedback (DFB) lasers and vertical-cavity surface-emitting lasers (VCSELs) where a highly directional light emission is desirable. For micro- or nano- lasers, the length scales of the lasing modes are usually comparable to or even smaller than the lasing wavelength.

Therefore, diffraction can occur in one or more dimensions, resulting in a non-directional lasing emission [21, 22]. One exception is the lattice plasmon SPASER which has a surface area on the order of millimeters [28]. In the lattice design, directional emission can be achieved. Spatial coherence on the millimeter scale and temporal coherence on the picosecond scale have been demonstrated in lattice devices [48].

(v) Mode volume. One motivation to develop plasmon lasers is to exploit their subwavelength mode volumes and employ them as nanoscale light sources that can be integrated with other devices. The SPASER design based on colloidal nanoparticles provides the smallest mode volume because of the natural spatial confinement of LSP resonances [39]. However, lasing with a single plasmonic nanoparticle has not been demonstrated. The smallest mode volume of a lasing plasmon demonstrated to date was achieved by the gap plasmon laser, which has a mode volume of approximately $\lambda_0^3/1000$, where λ_0 is the free-space wavelength, and is confined in the deep-subwavelength gap [22]. As a comparison, the mode volumes of both the lattice plasmon SPASER and the SPP lasers are around λ_0^3 [20, 28].

(vi) Modulation speed. Another advantage of nanoscale lasers is that they can be modulated at high rates because of their small mode volumes. This has been demonstrated experimentally by plasmon lasers using direct-bandgap semiconductors [42]. Modulation of the lasing wavelength is achieved by electrically injecting carriers into the gain medium. Decay dynamics on the sub-nanosecond time scale indicate that these plasmon lasers can be modulated in the gigahertz range [49].

4.4 Applications of plasmon lasers

The fundamental advantages of plasmonics can be used in a broad range of applications. The fundamental properties of plasmonic resonances include optical near-field enhancement, flexible tunability, and enhanced light-matter interactions. The development of plasmon lasers adds another new dimension, leading to active plasmonic devices with improved performance over their passive counterparts. For example, refractive index sensing is one important application. The lasing wavelength of a plasmon laser is very sensitive to the refractive index of the local dielectric environment. Liquid analytes with slightly different refractive indices can be differentiated when mixed with laser dye molecules and brought into the region of a lasing plasmonic mode via microfluidic channels [50]. The refractive index change introduced by gaseous analytes can also be detected [51], making plasmon lasers useful in sensing explosive materials (Fig. 5f). SPASER-based plasmon lasers have also been demonstrated as biological probes in ultra-small volumes [52].

5. Conclusion

In comparison to optical modes in a dielectric material, noble metals can provide much tighter confinement to electromagnetic waves in the form of surface plasmons. Such tight confinement has inspired a wide variety of applications desiring small mode volumes for enhanced light-matter interaction. In this encyclopedia article, one such sub-area in this field – plasmon lasers – which deals with generation of coherent radiation at the nanoscale was discussed. A summary of the fundamental physics associated with surface plasmons is provided. Subsequently, a discussion of the various types of plasmonic resonant cavities that form the building block for plasmon lasers is presented. Finally, based on these concepts of surface plasmons and plasmon resonators, a discussion is given of the various experimental implementations of plasmon lasers to date. Within this discussion, the various characteristic parameters that describe the performance metric of a laser of this type, along with various potential applications of a plasmon laser is presented. This article is meant to serve as an entry-level guide for students and researchers working in the general area of optics, photonics or electromagnetics, and who are interested in the area of plasmonics, and more specifically on light generation at the nanoscale using lasers that utilize the benefits of surface plasmons.

6. References

[1] T. W. Ebbesen, H. J. Lezec, H. F. Ghaemi, T. Thio, and P. A. Wolff, "Extraordinary optical transmission through sub-wavelength hole arrays," *Nature* **391**, 667 (1998).

[2] T. Xu, A. Agrawal, M. Abashin, K. J. Chau, and H. J. Lezec, "All-angle negative refraction and active flat lensing of ultraviolet light," *Nature* **497**, 470 (2013).

[3] J. B. Pendry, L. Martín-Moreno, and F. J. Garcia-Vidal, "Mimicking Surface Plasmons with Structured Surfaces," *Science* **305**, 847 (2004).

[4] R. F. Oulton, V. J. Sorger, T. Zentgraf, R.-M. Ma, C. Gladden, L. Dai, *et al.*, "Plasmon lasers at deep subwavelength scale," *Nature* **461**, 629 (2009).

[5] K. C. Y. Huang, M.-K. Seo, T. Sarmiento, Y. Huo, J. S. Harris, and M. L. Brongersma, "Electrically driven subwavelength optical nanocircuits," *Nature Photonics* **8**, 244 (2014).

[6] N. Yu, J. Fan, Q. J. Wang, C. Pflügl, L. Diehl, T. Edamura, *et al.*, "Small-divergence semiconductor lasers by plasmonic collimation," *Nature Photonics* **2**, 564 (2008).

[7] H. A. Atwater and A. Polman, "Plasmonics for improved photovoltaic devices," *Nature Materials* **9**, 205 (2010).

[8] A. Kristensen, J. K. W. Yang, S. I. Bozhevolnyi, S. Link, P. Nordlander, N. J. Halas, *et al.*, "Plasmonic colour generation," *Nature Reviews Materials* **2**, 16088 (2016).

[9] D. Schurig, J. J. Mock, B. J. Justice, S. A. Cummer, J. B. Pendry, A. F. Starr, *et al.*, "Metamaterial Electromagnetic Cloak at Microwave Frequencies," *Science* **314**, 977 (2006).

[10] N. Yu, P. Genevet, M. A. Kats, F. Aieta, J.-P. Tetienne, F. Capasso, *et al.*, "Light Propagation with Phase Discontinuities: Generalized Laws of Reflection and Refraction," *Science* **334**, 333 (2011).

[11] P. L. Stiles, J. A. Dieringer, N. C. Shah, and R. P. V. Duyne, "Surface-Enhanced Raman Spectroscopy," *Annual Review of Analytical Chemistry* **1**, 601 (2008).

[12] M. Righini, P. Ghenuche, S. Cherukulappurath, V. Myroshnychenko, F. J. García de Abajo, and R. Quidant, "Nano-optical Trapping of Rayleigh Particles and Escherichia coli Bacteria with Resonant Optical Antennas," *Nano Letters* **9**, 3387 (2009).

[13] J. Renger, R. Quidant, N. van Hulst, and L. Novotny, "Surface-Enhanced Nonlinear Four-Wave Mixing," *Physical Review Letters* **104**, 046803 (2010).

[14] J. A. Kong, *Electromagnetic Wave Theory*, John Wiley and Sons, 2005.

[15] L. Novotny and B. Hecht, *Principles of Nano-Optics*, Cambridge University Press, 2012.

[16] S. A. Maier, *Plasmonics: Fundamentals and Applications*, Springer US, 2007.

[17] S. Enoch and N. Bonod, *Plasmonics: From Basics to Advanced Topics*, Springer Berlin Heidelberg, 2012.

[18] S. J. P. Kress, F. V. Antolinez, P. Richner, S. V. Jayanti, D. K. Kim, F. Prins, *et al.*, "Wedge Waveguides and Resonators for Quantum Plasmonics," *Nano Letters* **15**, 6267 (2015).

[19] V. J. Sorger, R. F. Oulton, J. Yao, G. Bartal, and X. Zhang, "Plasmonic Fabry-Pérot Nanocavity," *Nano Letters* **9**, 3489 (2009).

[20] W. Zhu, T. Xu, H. Wang, C. Zhang, P. B. Deotare, A. Agrawal, *et al.*, "Surface plasmon polariton laser based on a metallic trench Fabry-Perot resonator," *Science Advances* **3**, e1700909 (2017).

[21] S. J. P. Kress, J. Cui, P. Rohner, D. K. Kim, F. V. Antolinez, K.-A. Zaininger, *et al.*, "A customizable class of colloidal-quantum-dot spasers and plasmonic amplifiers," *Science Advances* **3**, e1700688 (2017).

[22] R.-M. Ma, R. F. Oulton, V. J. Sorger, G. Bartal, and X. Zhang, "Room-temperature sub-diffraction-limited plasmon laser by total internal reflection," *Nature Materials* **10**, 110 (2010).

[23] E. Petryayeva and U. J. Krull, "Localized surface plasmon resonance: Nanostructures, bioassays and biosensing—A review," *Analytica Chimica Acta* **706**, 8 (2011).

[24] M. Piliarik, P. Kvasnička, N. Galler, J. R. Krenn, and J. Homola, "Local refractive index sensitivity of plasmonic nanoparticles," *Optics Express* **19**, 9213 (2011).

[25] K. A. Willets and R. P. V. Duyne, "Localized Surface Plasmon Resonance Spectroscopy and Sensing," *Annual Review of Physical Chemistry* **58**, 267 (2007).

[26] B. Pettinger, B. Ren, G. Picardi, R. Schuster, and G. Ertl, "Nanoscale Probing of Adsorbed Species by Tip-Enhanced Raman Spectroscopy," *Physical Review Letters* **92**, 096101 (2004).

[27] W. Zhou, Y. Hua, M. D. Huntington, and T. W. Odom, "Delocalized Lattice Plasmon Resonances Show Dispersive Quality Factors," *The Journal of Physical Chemistry Letters* **3**, 1381 (2012).

[28] W. Zhou, M. Dridi, J. Y. Suh, C. H. Kim, D. T. Co, M. R. Wasielewski, *et al.*, "Lasing action in strongly coupled plasmonic nanocavity arrays," *Nature Nanotechnology* **8**, 506 (2013).

[29] L. Shi, T. K. Hakala, H. T. Rekola, J. P. Martikainen, R. J. Moerland, and P. Törmä, "Spatial Coherence Properties of Organic Molecules Coupled to Plasmonic Surface Lattice Resonances in the Weak and Strong Coupling Regimes," *Physical Review Letters* **112**, 153002 (2014).

[30] G. Vecchi, V. Giannini, and J. Gómez Rivas, "Surface modes in plasmonic crystals induced by diffractive coupling of nanoantennas," *Physical Review B* **80**, 201401 (2009).

[31] A. Yang, Z. Li, M. P. Knudson, A. J. Hryn, W. Wang, K. Aydin, *et al.*, "Unidirectional Lasing from Template-Stripped Two-Dimensional Plasmonic Crystals," *ACS Nano* **9**, 11582 (2015).

[32] A. Rottler, M. Bröll, S. Schwaiger, D. Heitmann, and S. Mendach, "Tailoring of high-Q-factor surface plasmon modes on silver microtubes," *Optics Letters* **36**, 1240 (2011).

[33] J. Gu, Z. Zhang, M. Li, and Y. Song, "Mode characteristics of metal-coated microcavity," *Physical Review A* **90**, 013816 (2014).

[34] Y.-F. Xiao, C.-L. Zou, B.-B. Li, Y. Li, C.-H. Dong, Z.-F. Han*, et al.*, "High-Q Exterior Whispering-Gallery Modes in a Metal-Coated Microresonator," *Physical Review Letters* **105**, 153902 (2010).

[35] M. I. Stockman, "Spasers explained," *Nature Photonics* **2**, 327 (2008).

[36] M. Premaratne and M. I. Stockman, "Theory and technology of SPASERs," *Advances in Optics and Photonics* **9**, 79 (2017).

[37] M. Ayata, Y. Fedoryshyn, W. Heni, B. Baeuerle, A. Josten, M. Zahner, *et al.,* "High-speed plasmonic modulator in a single metal layer," *Science* **358**, 630 (2017).

[38] D. J. Bergman and M. I. Stockman, "Surface Plasmon Amplification by Stimulated Emission of Radiation: Quantum Generation of Coherent Surface Plasmons in Nanosystems," *Physical Review Letters* **90**, 027402 (2003).

[39] M. A. Noginov, G. Zhu, A. M. Belgrave, R. Bakker, V. M. Shalaev, E. E. Narimanov*, et al.*, "Demonstration of a spaser-based nanolaser," *Nature* **460**, 1110 (2009).

[40] N. I. Zheludev, S. L. Prosvirnin, N. Papasimakis, and V. A. Fedotov, "Lasing spaser," *Nature Photonics* **2**, 351 (2008).

[41] F. van Beijnum, P. J. van Veldhoven, E. J. Geluk, M. J. A. de Dood, G. W. ’t Hooft, and M. P. van Exter, "Surface Plasmon Lasing Observed in Metal Hole Arrays," *Physical Review Letters* **110**, 206802 (2013).

[42] R.-M. Ma, X. Yin, R. F. Oulton, V. J. Sorger, and X. Zhang, "Multiplexed and Electrically Modulated Plasmon Laser Circuit," *Nano Letters* **12**, 5396 (2012).

[43] Q. Zhang, G. Li, X. Liu, F. Qian, Y. Li, T. C. Sum*, et al.*, "A room temperature low-threshold ultraviolet plasmonic nanolaser," *Nature Communications* **5**, 4953 (2014).

[44] R. Chandrasekar, Z. Wang, X. Meng, S. I. Azzam, M. Y. Shalaginov, A. Lagutchev*, et al.*, "Lasing Action with Gold Nanorod Hyperbolic Metamaterials," *ACS Photonics* **4**, 674 (2017).

[45] T. Pickering, J. M. Hamm, A. F. Page, S. Wuestner, and O. Hess, "Cavity-free plasmonic nanolasing enabled by dispersionless stopped light," *Nature Communications* **5**, 4972 (2014).

[46] W. Holzer, H. Gratz, T. Schmitt, A. Penzkofer, A. Costela, I. García-Moreno*, et al.*, "Photo-physical characterization of rhodamine 6G in a 2-hydroxyethyl-methacrylate methyl-methacrylate copolymer," *Chemical Physics* **256**, 125 (2000).

[47] D. Wang, A. Yang, W. Wang, Y. Hua, R. D. Schaller, G. C. Schatz*, et al.*, "Band-edge engineering for controlled multi-modal nanolasing in plasmonic superlattices," *Nature Nanotechnology* **12**, 889 (2017).

[48] T. B. Hoang, G. M. Akselrod, A. Yang, T. W. Odom, and M. H. Mikkelsen, "Millimeter-Scale Spatial Coherence from a Plasmon Laser," *Nano Letters* **17**, 6690 (2017).

[49] T. P. H. Sidiropoulos, R. Röder, S. Geburt, O. Hess, S. A. Maier, C. Ronning*, et al.*, "Ultrafast plasmonic nanowire lasers near the surface plasmon frequency," *Nature Physics* **10**, 870 (2014).

[50] A. Yang, T. B. Hoang, M. Dridi, C. Deeb, M. H. Mikkelsen, G. C. Schatz*, et al.*, "Real-time tunable lasing from plasmonic nanocavity arrays," *Nature Communications* **6**, 6939 (2015).

[51] R.-M. Ma, S. Ota, Y. Li, S. Yang, and X. Zhang, "Explosives detection in a lasing plasmon nanocavity," *Nature Nanotechnology* **9**, 600 (2014).

[52] E. I. Galanzha, R. Weingold, D. A. Nedosekin, M. Sarimollaoglu, J. Nolan, W. Harrington, *et al.*, "Spaser as a biological probe," *Nature Communications* **8**,15528 (2017).

Acknowledgement

W. Z., S. D., M. S. D., C. Z. and A. A. acknowledge support under the Cooperative Research Agreement between the University of Maryland and the National Institute of Standards and Technology, Center for Nanoscale Science and Technology, Award#70NANB14H209, through the University of Maryland.